# Numerical Simulation of Shock Propagation in Bubbly Liquids by the Front Tracking Method

Can F. Delale[1,2], Selman Nas[1], and Gretar Tryggvason[3]

[1] Faculty of Aeronautics and Astronautics, Istanbul Technical University, 34469 Maslak, Istanbul, Turkey. delale@itu.edu.tr , nas@itu.edu.tr
[2] TÜBİTAK Feza Gürsey Institute P.O. Box 6, 81220 Çengelköy, Istanbul, Turkey. delale@gursey.gov.tr
[3] Department of Mechanical Engineering, Worcester Polytechnic Institute, 100 Institute Road, Worcester, MA 01609-2280, USA. gretar@wpi.edu

## 1 Introduction

The propagation of shock waves in bubbly liquids has attracted great interest because of its practical importance. It has many interesting applications in petroleum and chemical engineering, biological and medical sciences, geophysics, etc. It is also of fundamental importance. Despite the fact that shock waves in a dilute bubbly liquid have been extensively investigated in the literature [1-4] using model equations, direct numerical simulations using the full Navier-Stokes equations, where the effects of viscosity and vorticity are fully accounted for, have not been treated before due to the complexity of the phenomenon. The front tracking method [5], has been rather successful in solving the full Navier-Stokes equations in the presence of a deforming phase boundary in many multi-phase flow applications. Such applications [6,7] include the collapse of a cavitation bubble near a solid wall and the formation of a toroidal bubble by a high speed micro-jet near a rigid boundary.

Here, our goal is to extend the front tracking method to be able to follow the collapse of a cluster of bubbles in a quiescent liquid inside a 2D or 3D rectangular domain excited by a pressure jump (*shock wave*) at the top. The study of a relatively simple model (say, by considering a polytropic law for the gas as a first step) by direct numerical simulations (DNS) using the front tracking method, where bubble deformations and interactions are fully accounted for, is a useful first step in understanding the flow characteristics behind the shock. Such simulations will yield information about the magnitude of velocity and pressure fluctuations, and allow us to quantify the effect of bubble/bubble interactions and bubble deformation. Numerical simulations also make it possible to go beyond the classical Rayleigh-Plesset analysis for a dilute liquid, where the upper limit of the void fraction is only a few percent.

## 2 Shock Propagation in Bubbly Liquids by DNS using The Front Tracking Method

We consider a bubbly liquid filling a 2D or a 3D rectangular domain. The bubbles are initially assumed to be either circular (in 2D) or spherical (in 3D) in shape, uniformly distributed and in equilibrium with the surrounding liquid. A pressure jump (incident shock wave) is introduced at the top wall of the domain (with liquid inflow) and a wall boundary condition is imposed at the bottom (with no outflow). The domain is taken to be periodic in the transverse direction(s). For the numerical simulation by the front tracking method, the fluid motion is governed by the normalized unsteady Navier-Stokes equations, valid for the whole flow field. Neglecting gravity and surface tension, these equations can be written as

$$\frac{\partial(\rho \mathbf{u})}{\partial t} \; + \; \nabla . (\rho \, \mathbf{u} \, \mathbf{u}) \; = \; - \, \nabla \, p \; + \; \frac{1}{(Re)} \, \nabla . (2 \, \mu \, \mathcal{D}) \tag{1}$$

where the density $\rho$ varies in the interval $\rho_b \leq \rho \leq \rho_\ell$ and the viscosity $\mu$ varies in the interval $\mu_b \leq \mu \leq \mu_\ell$, with subscripts $b$ and $\ell$ denoting the bubble and the liquid, respectively. Here, $\mathcal{D}$ is the deformation tensor, $\mathbf{u}$ is the velocity field and $p$ is the pressure field. The Reynolds $Re$ number is given by

$$Re \; = \; \frac{\rho'_m \, \sqrt{p'_m / \rho'_m} \, L'}{\mu'_m} \tag{2}$$

where $L'$ is a characteristic length of the order of the initial mean radius of the bubbles, $\rho'_m$ and $\mu'_m$ are conveniently defined normalization values of the density and of the viscosity, both lying between those values of the liquid and of the bubble, and $p'_m$ is a normalization pressure chosen for a characteristic speed $\sqrt{p'_m / \rho'_m}$ or for a characteristic time $L' \, \sqrt{\rho'_m / p'_m}$ (all primed variables are dimensional). We neglect the compressibility of the carrier liquid, taking it to be incompressible so that

$$\nabla . \mathbf{u} \; = \; 0 \tag{3}$$

in the carrier liquid phase, and assuming its viscosity and density to remain constant at all times. The bubbles, on the other hand, are compressible with the pressure inside either set to a constant or varied isothermally. This imposes a moving boundary condition on the pressure field to be satisfied at the bubble/liquid interfaces and forces the imposed pressure at the top to drop to the level specified inside the bubbles. Thus, the presence of the bubbles prevents the effect of the increased pressure at the top to reach further into the bubbly mixture. The fact that the bubbles do not completely block the channel allows this effect to be felt slightly deeper, but not significantly. Equation (1), along with the incompressibility condition (3) in the carrier liquid phase and a specified pressure in the bubbles, set equal to either a global constant

or its local value resulting from the polytropic law, are solved iteratively by a conventional finite volume method on a staggered grid [5]. For the simulations with the polytropic gas law, we evaluate the area (2D) or volume (3D) of each bubble at each time step. The Reynolds number is assumed to be of $O(1)$ in magnitude characterizing a flow field with a finite, but low Reynolds number. Numerical simulations were carried out for both two- and three-dimensional domains. Since the pressure is specified inside the bubbles, the fluid properties there play a minor role in the evolution and to make the computations as easy as possible, we used a density and viscosity ratio of $\rho_\ell/\rho_b = \mu_\ell/\mu_b = 10$. Tests with higher ratios using the two-dimensional domain confirmed that the results are essentially independent of these ratios. The computed results were compared with those of one-dimensional homogeneous bubbly mixture theory. In particular, a mean shock speed was found by computing the distances advanced by a constant pressure rise in the shock profile over a time interval $\Delta t$ at several times during the evolution and by dividing the mean distance by $\Delta t$. The shock speeds thus obtained were compared with those calculated by the one-dimensional homogeneous bubbly liquid theory where the shock speeds $U_s$ are given by

$$U_s^2 \;=\; \frac{(1\,-\,\beta_1)(p_1\,-\,p_0)}{(1\,-\,\beta_0)\,(\beta_0\,-\,\beta_1)\,\rho_\ell} \quad , \tag{4}$$

using the Rankine-Hugoniot relations[1,2] at a discontinuity connecting two regions of equilibrium states, designated by 0 and 1. In eq. (4), $\beta_0$ and $\beta_1$ are the void fractions and $p_0$ and $p_1$ are the mixture pressures of the equilibrium regions 0 and 1, respectively. To justify the comparison of the mean shock speed with eq. (4), steady-state conditions for shock propagation should be reached which require long distances in the direction of propagation[9,10]. Although these conditions are probably not reached over the relatively short distances of propagation in the computational domains of the present simulations, the calculated r.m.s. values of fluctuations of the instantaneous shock speeds about the mean shock speed are shown to be only within a few percent, making the comparison of the mean shock speed with eq. (4) meaningful.

## 3 Results and Discussion

For the numerical simulations, two- and three-dimensional rectangular computational domains were considered. A grid study was conducted with a resolution ranging from 50 × 98 points to 122 × 242 points in 2D and from 18 × 18 × 66 points to 34 × 34 × 130 points in 3D in order to control numerical accuracy. Better resolution of the bubble/liquid interfaces were observed as the grid resolution was increased. However, the results for the shock structures and shock speeds remained almost unchanged. For the 2D case,where the gas pressure inside the bubbles is held constant, a rectangular grid containing 24

bubbles were considered. All bubbles were assumed to be initially circular in shape with the same radius $R = 0.25$. At time zero, the pressure at the top of the domain was raised by $\Delta p = 0.4$ and kept constant during the simulations.

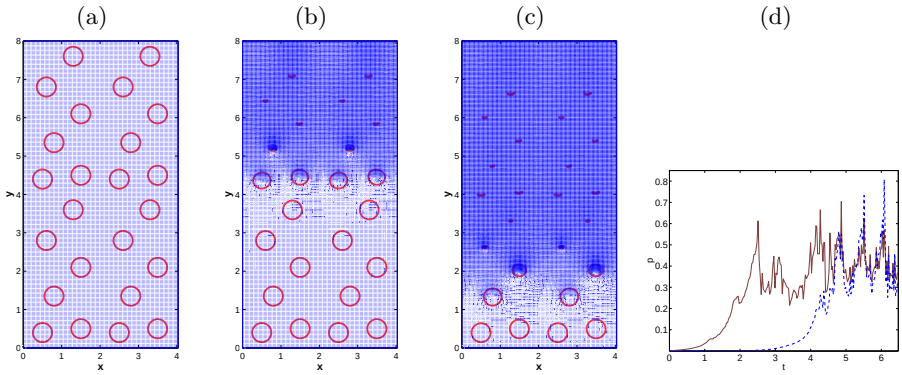


**Fig. 1.** Results obtained by the front tracking method showing a shock wave initially at $y = 8.0$ with strength $\Delta p = 0.4$ propagating into a quiescent bubbly liquid in a rectangular domain containing 24 bubbles, each with initial radius $R = 0.25$ where the gas pressure inside the bubble is held constant at its initial value (the density and viscosity of the liquid and of the gas are, respectively, $\rho_\ell = 2.5$ ; $\mu_\ell = 0.07$ and $\rho_b = 0.25$ ; $\mu_b = 0.007$). **(a)** Snapshot of the bubbly liquid at the initial time $t = 0.0$. **(b)** Snapshot of the bubbly liquid at time $t = 3.0$ showing the collapse of bubbles as the shock propagates (shaded areas show higher pressure zones). **(c)** Snapshot of the bubbly liquid at time $t = 5.5$ showing the collapse of bubbles as the shock propagates (shaded areas show higher pressure zones). **(d)** The pressure distribution for the bubbly shock wave at locations $y = 3.333$ (dashed line) and $y = 6.0$ (solid line) along the boundary $x = 0$.

Snapshots of the results obtained by the front tracking method showing the deformation of the collapsing bubbles and the evolution of the pressure distribution at two locations along the direction of propagation (the $y$-axis) in a rectangular grid with a resolution of $122 \times 242$ points are shown in Figs. 1 (a)-(d). The results in Figs. 1 (a)-(c) show that the bubbles collapse with non-circular shape (almost elliptical in the beginning) followed by a re-entrant jet before they totally disappear (the interfaces are here resolved up to a point where the top interface almost touches the bottom one). In this case, the fluctuations in the hydrodynamic variables observed in the transverse direction ($x$-direction) are reasonably small to justify the use of the one-dimensional homogeneous bubbly flow theory. Figure 1 (d) shows the evolution of the pressure distribution of oscillating shock waves at locations $y = 3.333$ and $y = 6.0$ along the direction of propagation ($y$-axis) at the boundary $x = 0$, where periodic boundary conditions are imposed. The amplitude of the pres-

sure fluctuations in this case can be as high as 0.36 at the beginning of oscillations, but they eventually decay in time. The mean shock speed obtained by the simulations using the above mentioned averaging yields a value equal to 1.103 (with r.m.s. fluctuations being less than 2%), which seems to be in good agreement with the value $U_s = 1.128$ evaluated by eq. (4) for homogeneous bubbly liquids with $p_1 - p_0 = \Delta p = 0.4$, $\rho_\ell = 2.5$, $\beta_0 = 0.1473$ and $\beta_1 = 0.0$.

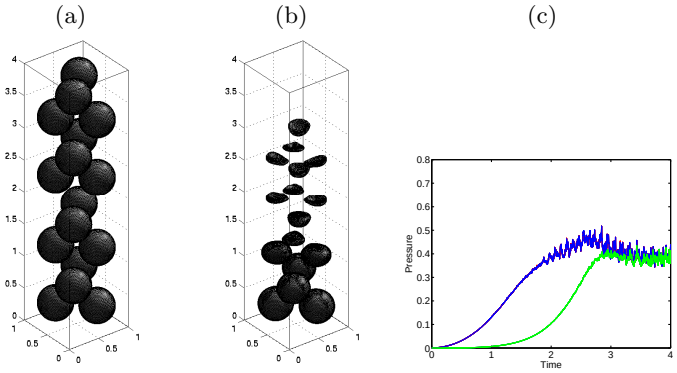


**Fig. 2.** Results obtained by the front tracking method showing a shock wave with strength $\Delta p = 0.4$ propagating into a quiescent bubbly liquid in a rectangular box containing 16 bubbles, each with initial radius $R = 0.25$ where the gas pressure inside the bubble is held constant at its initial value. **(a)** Snapshot of the bubbly liquid at the initial time $t = 0.0$. **(b)** Snapshot of the bubbly liquid at time $t = 3.5$ showing the non-spherical collapse of bubbles as the shock propagates. **(c)** The pressure distribution for the bubbly shock wave at locations $z = 2.0$ (light line) and $z = 3.0$ (dark line) along the line $x = 0$ and $y = 0$.

The 3D numerical simulations for the case where the gas pressure was held constant were carried out in a rectangular box, with a grid resolution of $34 \times 34 \times 130$ points, containing 16 bubbles. The bubbles were again taken initially in equilibrium with the quiescent liquid and spherical in shape, all with the same radius $R = 0.25$. A shock wave with strength $\Delta p = 0.4$ was incident at the top wall of the rectangular box. The results obtained by the front tracking method are shown in Figs. 2 (a)-(c). The non-spherical collapse of bubbles as the shock propagates can clearly be seen in Fig. 2 (b). An almost uniform flow field can be observed over the cross-section in the lateral direction as the shock propagates, justifying the use of eq. (4) for the one-dimensional homogeneous bubbly liquid model in this case as well. The pressure distributions at locations $z = 2.0$ and $z = 3.0$ along the line $x = 0$ and $y = 0$ in the propagation direction of the shock are plotted in Fig. 2 (d). The pressure fields at these locations oscillate with a maximum

amplitude of 0.15, and the pressure fluctuations decay as the shock propagates further. The mean shock speed from the simulations using the above discussed averaging method yields a value of 0.953 (with r.m.s. fluctuations being less than 5%), which seems to agree well with the value $U_s = 0.91$ evaluated by eq. (4) for homogeneous bubbly liquids with $p_1 - p_0 = \Delta p = 0.4$, $\rho_\ell = 2.5$, $\beta_0 = 0.2618$ and $\beta_1 = 0.0$.

Finally, a 2D numerical simulation was carried out for the case where a 2D isothermal law (with the polytropic index being equal to unity ) for the gas pressure was assumed. The same rectangular grid used for the constant pressure case containing 24 bubbles, all having the same radius $R = 0.25$, was considered for the flow simulations. The incident shock strength was also set equal to $\Delta p = 0.4$ to allow a full comparison with the case of constant gas pressure. Snapshots of the initial bubble distribution and of its evolution using a grid resolution of $122 \times 242$ points at non-dimensional times $t = 1.6$ and $t = 3.6$ are shown in Figs. 3 (a)-(c).

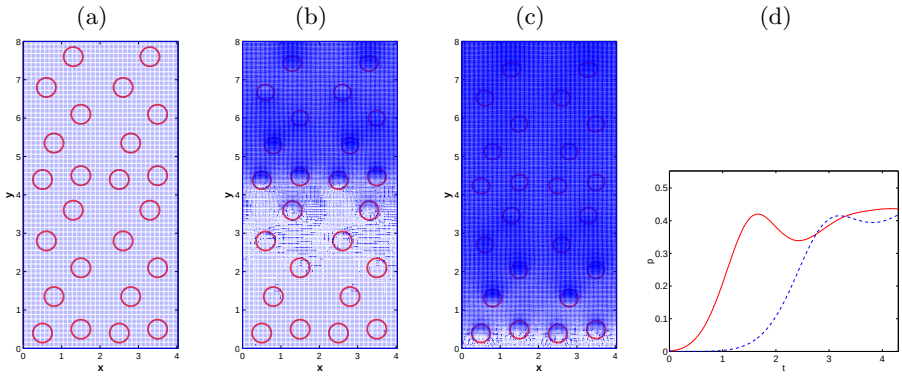


**Fig. 3.** Results obtained by the front tracking method showing a shock wave with strength $\Delta p = 0.4$ propagating into a quiescent bubbly liquid in a rectangular domain containing 24 bubbles, each with initial radius $R = 0.25$ where the gas pressure is varied isothermally (the density and viscosity of the liquid and of the gas are, respectively, $\rho_\ell = 2.5$ ; $\mu_\ell = 0.07$ and $\rho_b = 0.25$ ; $\mu_b = 0.007$). **(a)** Snapshot of the bubbly liquid at the initial time $t = 0.0$. **(b)** Snapshot of the bubbly liquid at time $t = 1.6$ showing collapsing bubbles behind the shock as the shock propagates (shaded areas show higher pressure zones). **(c)** Snapshot of the bubbly liquid at time $t = 3.6$ showing collapsing and rebounding bubbles behind the shock as the shock propagates (shaded areas show higher pressure zones). **(d)** The pressure distribution for the bubbly shock wave at locations $y = 3.333$ (dashed line) and $y = 6.0$ (solid line) along the boundary $x = 0$.

The initial void fraction is 0.1473 and the void fractions behind the shock at $t = 1.6$ and $t = 3.6$ are, respectively, 0.1114 and 0.096, showing an overall decrease in the void fraction as the shock propagates. Relatively small

changes in the movement of the bubble centers are observed implying that the motion of the bubble centers can be neglected. When the shock front hits the boundary of the bubbles, the bubbles start to collapse isothermally and the gas pressure inside the bubbles increases resulting in a decrease in the pressure threshold for further collapse. Eventually this pressure threshold diminishes and the bubbles rebound (after a few oscillations, they would eventually reach equilibrium if the computational domain could have been enlarged). Therefore, in the first instance of shock propagation, only collapsing bubbles are seen (Fig. 3(b)). As the shock propagates downward towards the bottom wall, the bubbles close to the top (where the shock was incident) start to rebound (Fig. 3 (c)). The bubble collapses and rebounds are seen to be almost elliptical in shape for this case. Again, the lateral pressure and velocity fluctuations can be neglected resulting in an almost one-dimensional propagation of the shock front. The evolution of the pressure distributions at locations $y = 3.333$ and $y = 6.0$ along the boundary, where periodic boundary conditions are imposed, are shown in Fig. 3 (d). The profiles look much more smooth for the reasons explained above. The mean shock speed obtained from the simulations using the above mentioned averaging yields a value of 1.992 (with r.m.s. fluctuations being less than 7%). On the other hand, the shock speed $U_s$ of one-dimensional homogeneous bubbly liquid is evaluated by eq. (4) with $\rho_\ell = 2.5$, $p_1 - p_0 = \Delta p = 0.4$ , $\beta_0 = 0.1473$ and $\beta_1 = \beta_0/(1 + \Delta p) = 0.1052$. The shock speed thus obtained using eq. (4) yields the value $U_s = 1.997$, which agrees well with the simulated value. Due to the increase in the gas pressure as the bubbles collapse, the bubbles collapse at a slower rate and the shock propagates faster in this case as compared to the case where the gas pressure is held constant under the same conditions.

## 4 Concluding Remarks

The results of this investigation have shown that shock propagation in a bubbly liquid with void fractions as high as 15% to 25% can still be well described by the one-dimensional homogeneous bubbly liquid model when the gas pressure inside the bubble is kept constant or varied isothermally, irrespective of the dimensionality of the computation domain. While bubble deformation and bubble/bubble interactions are properly accounted for by the present simulations, our results do not address the effects of liquid compressibility, thermal damping and bubble fragmentation. These effects demand the solution of the compressible Navier-Stokes equations together with the energy equation both inside and outside the bubble. Although this does not seem to be possible at present times, a model equation that replaces the polytropic law for the pressure inside the bubble by an equation similar to that proposed by Prosperetti [8] to take into account the effect of thermal damping can be used as a first step. Only then, can this simple model be extended to simulate bubbly flows in more complex geometries than those examined here, such as bubbly flows

through constrictions or over curved boundaries.

**Acknowledgements**

This work was supported in part by the US Department of Energy under grant no. DE-FG02-03ER46083 and in part by the Research Foundation of Istanbul Technical University (BAP) under Project No. 1874 .

## References

1. Noordzij L, van Wijngaarden L (1974) J.Fluid Mech. 66:115-143.
2. Beylich AE, Gülhan A (1990) Phys. Fluids A 2:1412-1428.
3. Watanabe M, Prosperetti A (1994) J. Fluid Mech. 274:349-381.
4. Kameda M, Shimaura N, Higashino F and Matsumoto Y (1998) Phys. Fluids 10:2661-2668.
5. Tryggvason G, Bunner B, Esmaeeli A, Juric D, Al-Rawahi N, Tauber NW, Hans J, Nas S, Jan, YJ (2001) J. Comput. Phys. 169:662-682.
6. Yu PY, Ceccio SL, Tryggvason G (1995) Phys. Fluids 7:2608-2616.
7. Popinet S, Zaleski S (2002) J. Fluid Mech. 464:137-163.
8. Prosperetti A (1991) J. Fluid Mech. 222:587-616.